ISSN:2790-1688 Volume-11-(2024)

Stability Analysis of Yebatan Underground Cavern Surrounding Rock based on Crack Evolution Theory

Xianglin Xing [1,a], Li Qian [2,b], Guoyan Zhang [2,c], Jianhai Zhang [2,d]

[1] Power China Chengdu Engineering Corporation Limited, Chengdu, China

[2] College of Water Resources and Hydropower, State Key Laboratory of Hydraulics and Mountain River Engineering, Sichuan University, Chengdu, China

[a] 414872545@qq.com, [b] scu_ql91@163.com, [c] 289021561@qq.com, [d] zhangjianhai@scu.edu.cn

Abstract. The deformation properties of rock are closely related to the effect of crack closure, generation and expansion in the rock. In this paper, the stress-crack strain evolution constitutive model is used to determine the relaxation damage zone of the surrounding rock based on the change regulation of the crack closure ratio during the whole process of surrounding rock damage, and the model is embedded into FLAC3D software, and then the stability evaluation of the surrounding rock of the cavern group under unsupported and supported conditions is carried out for the underground plant of Yebatan hydropower station. The excavation simulation shows that the displacement of the cavern surrounding rock increases with the excavation step, and the influence of the fault on the displacement of the surrounding rock is very significant. The high stress concentration area is distributed in the arch top of the plant, the tailwater connection hole, the arch top and the bottom of the tail chamber, and the tensile stress area is mainly distributed in the high side wall of the underground plant and the tail chamber. The crack closure ratio index was used to quantitatively evaluate the degree of relaxation damage of the surrounding rock, indicating that the relaxation damage area is influenced by the fault, and the volume of the surrounding rock damage area under the system support is significantly reduced compared with the unsupported working condition, showing the effectiveness of the support measures.

Keywords: rock crack evolution, underground cavern, surrounding rock stability, Yebatan, relaxation zone.

1. Introduction

The crack evolution of the rock has an important influence on the deformation and stability of the underground cavern group surrounding rock excavation. The deformation properties of the underground cavern are closely related to the closure, generation and expansion of crack in the rocks. Many scholars have devoted themselves to the study of crack generation and extension[1-5]. Wen[6] proposed a damage constitutive model considering the crack closure effect, which can more reasonably reflect the damage evolution of the rock during the deformation of the crack closure stage. Mo[7] used rock triaxial compression tests and multistage creep tests to reveal the crack strain evolution characteristics, and proposed Mo's model, which represents both the transient and time-dependent mechanical properties of the micritic bioclastic limestone. Xu [8] established a statistical constitutive model for thermal damage of rocks under triaxial compression conditions by combining statistics and damage theory. The damage evolution curves reflect the whole process of closure, generation, extension, penetration of rock microcracks. It provides a valuable reference for the study of rock deformation and stability in deep engineering. Qian[9] obtained the expressions of axial crack strain and lateral crack strain for each stage of crack evolution through the analysis of five stages of crack evolution of Shuangjiangkou granite, and established a stress-crack strain evolution constitutive model.

These studies show that it is important to consider the evolution of rock cracks in order to reflect the mechanical behaviour of rocks. Therefore, in this paper, the stress-crack strain evolution constitutive model[9] is used and embedded into FLAC3D software to simulate the excavation of the underground plant of Yebatan hydropower station in unsupported condition and system

supported condition to study the excavation deformation and disturbance damage regulation of the surrounding rock and evaluate the stability of the surrounding rock excavation.

2. Stress-crack strain evolution constitutive model

As shown in Figure 1, granite crack evolution includes five stages[10-13]: crack closure stage (stage I), elastic stage (stage II), crack stable growth stage (stage III), crack unstable growth stage (stage IV), and crack post-peak stage (stage V). σ_{cc} , σ_{ci} , σ_{cd} , and σ_p are the threshold stresses in stage I, stage II, stage III, and stage IV, respectively. ε_1^{cc} , ε_1^{ci} , ε_1^{cd} , ε_1^{cp} and, ε_3^{ci} , ε_3^{cd} , ε_3^{cp} are the axial crack strains and lateral crack strains corresponding to the threshold stresses.

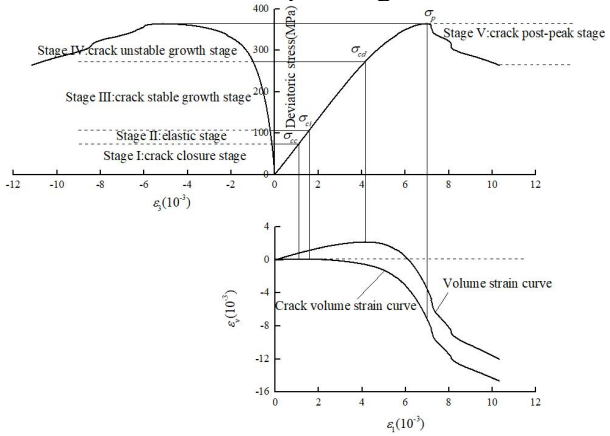

Fig.1 Granite cracking evolution

The ratio of the deviatoric stress to the peak strength, Rd [14], can be expressed as:

$$R_d = \frac{\sigma_1 - \sigma_3}{\sigma_p} \tag{1}$$

where $\sigma_1 - \sigma_3$ is the deviatoric stress, σ_p is the peak strength, the deviatoric stress at Rd =1.

According to the above definition of Rd, R_d^{cc} , R_d^{ci} , R_d^{cd} are the ratio of σ_{cc} , σ_{ci} , σ_{cd} to the peak stress, R_d^f is the ratio of failure stress to the peak stress.

The axial and lateral crack closure ratio C1 and C3 can be expressed as:

$$C_i = \begin{cases} \dfrac{\varepsilon_i^c}{\varepsilon_i^{cc}} & (0 \le R_d \le R_d^{cc} \ \ and \ \ \Delta R_d > 0) \\ 1 & (R_d^{cc} < R_d \le R_d^{ci} \ \ and \ \ \Delta R_d > 0) \\ 1 - \dfrac{\varepsilon_i^c - \varepsilon_i^{ci}}{\varepsilon_i^{cd} - \varepsilon_i^{ci}} & (R_d^{ci} < R_d \le 1 \ \ and \ \ \Delta R_d > 0) \\ 1 - \dfrac{\varepsilon_i^c - \varepsilon_i^{ci}}{\varepsilon_i^{cd} - \varepsilon_i^{ci}} & (R_d^f \le R_d < 1 \ \ and \ \ \Delta R_d \le 0) \end{cases} \tag{2}$$

where *i* is 1 or 3.

The stress-crack strain evolution constitutive model for full process of rock damage evolution is:

$$\Delta\sigma_i = \mathbf{D}^e(\Delta\varepsilon_i - \Delta\varepsilon_i^c) \tag{3}$$

Where, $\Delta\sigma_i$ is the three normal stress increments and three tangential stress increments of the model cell, $\Delta\varepsilon_i$ is the total strain increment in normal directions and the total tangential strain increment, $\Delta\varepsilon_i^c$ is the crack strain increment in 3 directions and the crack tangential strain

increment in 3 directions, i=1-6, $\mathbf{D}^e$ is the matrix of elastic constants, $\mathbf{D}^e$ and $\Delta\varepsilon_i^c$ can respectively be expressed as:

$$\mathbf{D}^e=\begin{bmatrix}\frac{E(1-\mu)}{(1-2\mu)(1+\mu)} & \frac{E\mu}{(1-2\mu)(1+\mu)} & \frac{E\mu}{(1-2\mu)(1+\mu)} & & & \\ \frac{E\mu}{(1-2\mu)(1+\mu)} & \frac{E(1-\mu)}{(1-2\mu)(1+\mu)} & \frac{E\mu}{(1-2\mu)(1+\mu)} & & & \\ \frac{E\mu}{(1-2\mu)(1+\mu)} & \frac{E\mu}{(1-2\mu)(1+\mu)} & \frac{E(1-\mu)}{(1-2\mu)(1+\mu)} & & & \\ & & & \frac{E}{1+\mu} & & \\ & & & & \frac{E}{1+\mu} & \\ & & & & & \frac{E}{1+\mu}\end{bmatrix} \tag{4}$$

$$\Delta\varepsilon_i^c=\begin{cases}\dfrac{-\Delta R_d\varepsilon_i^{cc}[1-\exp(-R_d/\eta_i^{cc})]}{\eta_i^{cc}} & (0\le R_d\le R_d^{cc}\ \ and\ \ \Delta R_d>0)\\ 0 & (R_d^{cc}<R_d\le R_d^{ci}\ \ and\ \ \Delta R_d>0)\\ \dfrac{\Delta R_d(\varepsilon_i^{cd}-\varepsilon_i^{cc})\exp[(R_d-R_d^{cd})/\eta_i^{cd}]}{\eta_i^{cd}} & (R_d^{ci}<R_d\le R_d^{cd}\ \ and\ \ \Delta R_d>0)\\ -\dfrac{\Delta R_d C_i^p(\varepsilon_i^{cd}-\varepsilon_i^{cc})\exp[(R_d-1)/\eta_i^p]}{\eta_i^p} & (R_d^{cd}<R_d\le 1\ \ and\ \ \Delta R_d>0)\\ \dfrac{k_i(\varepsilon_i^{cd}-\varepsilon_i^{cc})(C_i^f-C_i^p)\Delta R_d}{1-R_d^f} & (R_d^f\le R_d<1\ \ and\ \ \Delta R_d\le 0)\end{cases} \tag{5}$$

Where, η_1^{cc}, η_3^{cc}, η_1^{cd}, η_3^{cd}, η_1^{p}, η_3^{p} are the quasi-viscosity coefficients in the stage I, III, and IV, and k1, k3 are the stiffness coefficients of the elastic element in the stage V. These constitutive parameters can be determined by tri-axial compressive tests.

3. Zoning criterion of Yebatan underground rock relaxation damage

By conducting triaxial compression tests on the granite of Yebatan hydropower station, the stress-strain curves of the granite under different confining pressures were obtained. Based on the stress-crack strain evolution constitutive model described in the previous section, the identification of parameters for each crack evolution stage of the Yebatan granite was carried out [15], and the parameters of the constitutive model can be obtained as shown in Tab.1.

Table 1. Parameters of stress-crack strain evolution constitutive model

η_1^{cc}	η_3^{cc}	η_1^{cd}	η_3^{cd}	η_1^{p}	η_3^{p}	k_1	k_3
0.0781	0.0766	0.1179	0.1625	0.0521	0.0410	0.8683	0.9757

Figure 2 shows the relationship between crack closure ratio Ci and Rd when σ 3=1MPa. In the stage I, Ci gradually changes from 0 to 1 as the axial pressure increases. In the stage II, Ci is 1 and remains constant. In the stage III, Ci gradually decreases from 1 to 0. In the stage IV and V, Ci continuously decreases below 0.

It can be seen that Ci can quantitatively describe the state the surrounding rock. Either the axial crack closure ratio C1 or lateral crack closure ratio C3 can accurately and effectively describe the mechanism of crack development, and in the stage IV, the rock expansion is significant, and C3 shows better for the lateral expansion phenomenon.

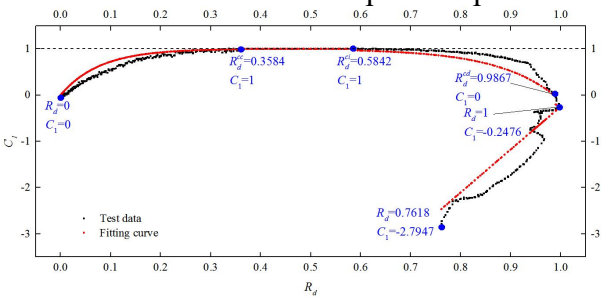

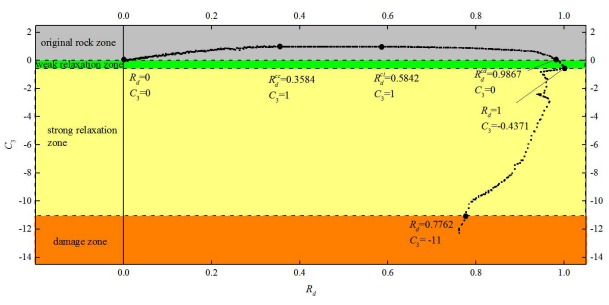

(a) C_1 vs R_d (b) C_3 vs R_d

Fig. 2 Relationship between C_i and R_d when σ_3=1MPa

Figure 3 shows the relationship between the apparent Poisson's ratio and Rd in the low (1 MPa), medium (20 MPa) and high (40 MPa) confining pressure in the stage IV and stage V. The apparent Poisson's ratio increases when Rd increases in the stage IV and increases when Rd decreases in the stage V, indicating that the lateral crack extension is the main reason for the occurrence of damage in the rock.

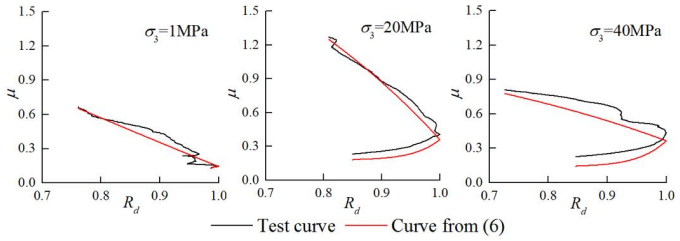

Fig. 3 Apparent Poisson's ratio versus R_d

When $R_d = R_d^{cd}$, the crack closure ratio inside the rock is the same as the rock in the natural state, C3=0 is the threshold when the rock crack turns from closure to extension. When $R_d > R_d^{cd}$, the rock enters the stage IV, and the strain of the rock increases rapidly until Rd =1the rock fails and damages, at this time, C3=-0.4371. Therefore, the rock with C3 $\geqslant$ 0 is considered to be in the original rock zone, the rock is in the weak relaxation zone when C3 is at [-0.4317,0). Since the specimen fails completely at C3=-12.2434, the rock with C3<-11 after excavation is considered as the damage zone for engineering safety reasons, and the rock is in the strong relaxation zone when C3 is at [-11,-0.4317).

In summary, the rock relaxation damage zone standard for the surrounding rock are determined in Tab.2, in which the rock integrity coefficients Kv is also given for different relaxation damage zones:

Table 2. rock relaxation damage zone standard

	original rock zone	weak relaxation zone	strong relaxation zone	damage zone
C_3	≥0	[-0.4317,0)	[-11,-0.4317)	<-11
K_v	>0.75	0.75~0.55	0.55~0.35	0.35~0.15

C3 can be used to divide the relaxation damage zone of the surrounding rocks of Yabatan into four zones, the damage zone, the strong relaxation zone, the weak relaxation zone and the original rock zone, as shown in Figure 2.

The stress-crack strain evolution constitutive model was embedded into FLAC3D through secondary development, and the stress-strain curves of the Yebatan rock specimens were numerically simulated under different confining pressures. The axial stress-strain and volume deformation curves are given in Figure 4. It can be seen that the experimental and numerical simulation curves are in agreement with each other, indicating that the constitutive model can be used for the calculation and analysis of the excavation simulation of the underground plant at Yebatan.

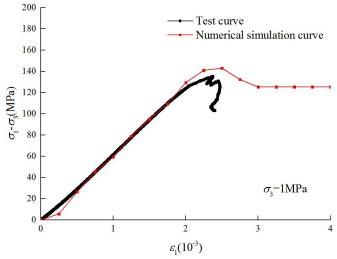

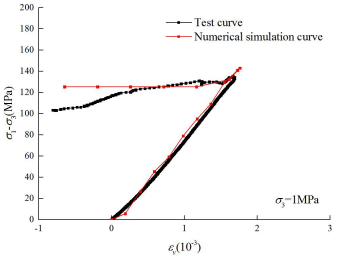

(a) Axial stress-strain curves (b) Volume stress-strain curves

Fig. 4 Test curves vs. numerical simulation curves of granite specimens under different confining pressure.

4. Calculation model and parameters

The numerical simulation range of the underground plant of Yebatan is shown in Figure 5. The X-direction is intercepted from the upstream main plant to the tail chamber, and the total length of the X-direction is 500m; the Y-direction is intercepted from unit 1 to unit 6, and the total length of the Y-direction is 500m; the bottom of the Z-direction is taken from the ▽2600.0m altitude, and the top extends to the top of the mountain. The entire 3D numerical model of Yebatan underground plant cavern group is shown in Figure 5(a), and Figure 5(b)(c) show the relationship between underground plant cavern group and faults. The model is divided into 611,487 elements, with a total of 274,261 nodes.

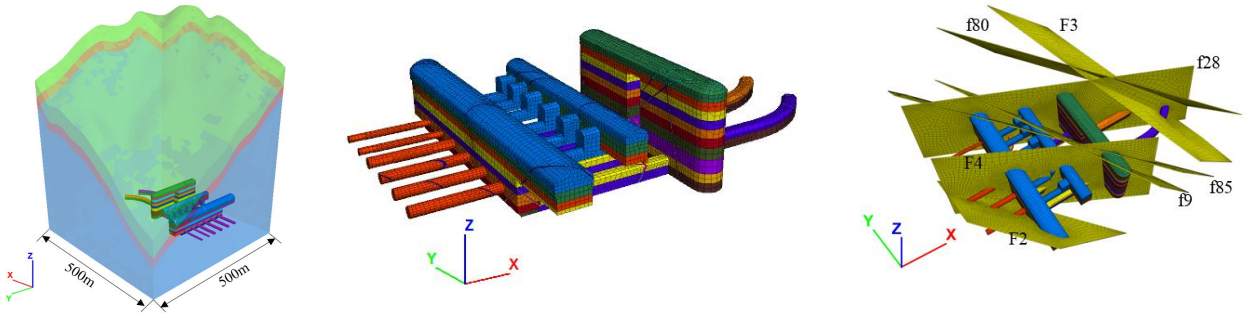

(a)3D model of the entire Yebatan underground plant

(b)Three-dimensional view of the cavern group

(c)Three-dimensional view of the cavern group and faults

Fig.5 Model of the underground plant cavern in Yebatan

Figure 6 shows the detailed procedures for the downward excavation. In the numerical calculation, the anchor is simulated by using the structural unit cable element in FLAC3D software, Φ 32L=9m, 1.2m × 1.2m arrangement, and the three-dimensional diagram of anchor support is given in Figure 7.

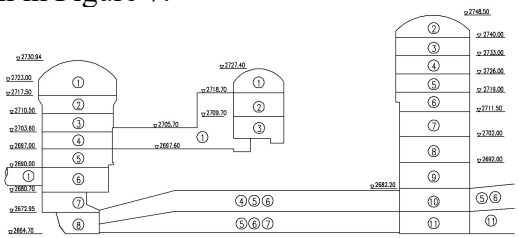

Fig. 6 Specific stratified excavation scheme of the Yebatan cavern group

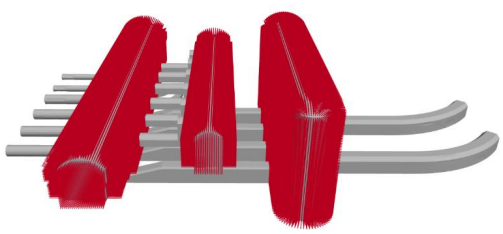

Fig. 7 3D diagram of anchor support

The values of parameters η_1^{cc}, η_3^{cc}, η_1^{cd}, η_3^{cd}, η_1^{p}, η_3^{p}, k1, k3 are shown in Tab.1. For the fault, the Mohr-Coulomb criterion is still used for simulation, and its parameters are shown in Tab.3. The anchor support parameters are shown in Tab.4.

Table 3. Strength parameters of the surrounding rock of Yebatan

Rock code	E （GPa）	Poisson's ratio μ	Density t/m^3	Coefficient of internal friction for shear strength f'	Cohesion （MPa）
III	13.0	0.20	2.72	1.08	1.10
IV	2.5	0.33	2.67	0.70	0.60
V	0.9	0.36	2.62	0.50	0.20
fault	0.2	0.36	2.23	0.35	0.05

Table 4. Anchor support parameters

Elastic modulus(GPa)	Slurry bonding strength （MPa）	Tensile yield strength （MPa）	Cement slurry stiffness （GPa）
200	1e14	1e14	10

5. Stability analysis and evolution of the crack damage zone of underground plant

5.1 The displacement of the surrounding rock

Figure 8 shows the deformation characteristics of the cavern group with graded excavation under unsupported and system support conditions in the form of three-dimensional diagrams, and Figure 9 shows the displacement distribution characteristics of unit 1# section and unit 4# section after excavation completion under unsupported and system support conditions.

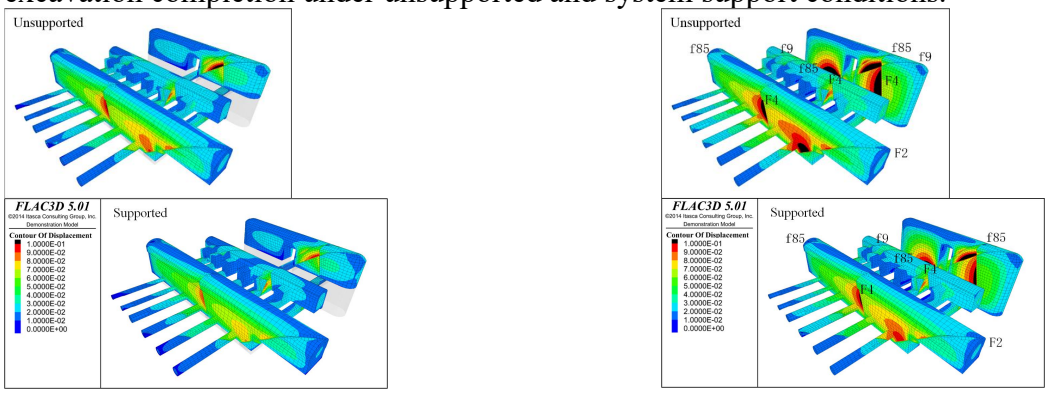

(a) VI layer excavation (b) XI layer excavation

Fig. 8 Distribution characteristics of deformation (unit:m) of excavated cavern group

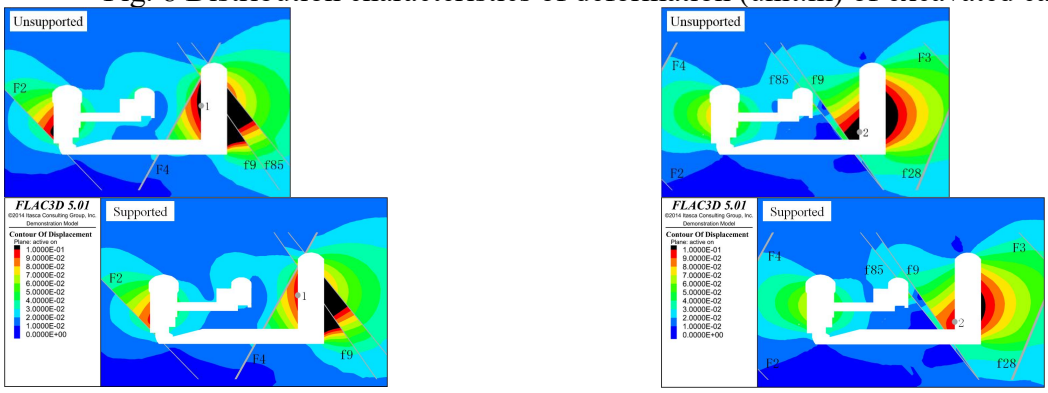

(a) unit 1# section(0+018.20m) (b) unit 4# section(0+111.80m)

Fig. 9 Displacement (unit:m) distribution characteristics after the XI layer excavation

It can be seen that with undergoing of excavation, the change of the displacement of the surrounding rock of the three major cavern chambers gradually increases, and after the I layer excavation, the displacement of the cavern is about 10-30mm, while after the VI layer excavation, the extreme value of the displacement of the cavern increases to about 100mm, and the extreme value of the displacement after the XI layer excavation is greater than 100mm, especially the parts affected by faults.

The deformation regulation of the surrounding rock of the underground cavern group before and after reinforcement is consistent, and the deformation magnitude and scope of the parts affected by the fault F2, F4, f9, f85, etc. are significantly increased, especially the deformation of the side walls of the main plant and the tail chamber greater than 100mm are directly related to the fault, reflecting the obvious structural surface control type deformation characteristics.

The areas where the displacement of the underground cavern in the unit 1# section is more than 100mm are mainly located in the area where the side wall of the main plant is affected by fault F2 and the area near the high side wall of the tail chamber is affected by faults F2, f9 and f85. The areas where the displacement of the underground cavern in the unit 4# section is more than 100mm are mainly located in the area where the high side wall of the tail chamber and the nearby area is affected by fault f9.

The displacement of the underground cavern was reduced after reinforcement, for example, the displacement of point 1 in Figure 9 was reduced from 99.39mm to 89.25mm after reinforcement; the displacement of point 2 in Figure 9 was reduced from 109.23mm to 95.21mm after reinforcement.

5.2 Stress distribution in the surrounding rock

Figure 10 and Figure 11 show the maximum and minimum principal stress distribution characteristics of the unit 1# section and unit 4# section after the XI layer excavation under unsupported condition and system support condition respectively. It can be seen:

The high stress concentration area is distributed in the arch top of the plant, the tailwater connection hole, the arch top and the bottom of the tail chamber.The tensile stress zone of the underground cavern in the unit 1# section is mainly distributed in the area affected by fault F2 in the upstream side wall of the main plant and the area affected by faults F2, f9 and f85 near the high side wall of the tailing chamber. The tensile stress zone of the underground cavern in the unit 4# section is mainly distributed at the bottom of the high side wall upstream of the main plant, the part of the side wall downstream of the main transformer room affected by fault f85 and the part of the high side wall upstream of the tail chamber and the part nearby affected by fault f9. The range (black part in Figure 11) and depth of the tensile stress zone are obviously affected by the faults.

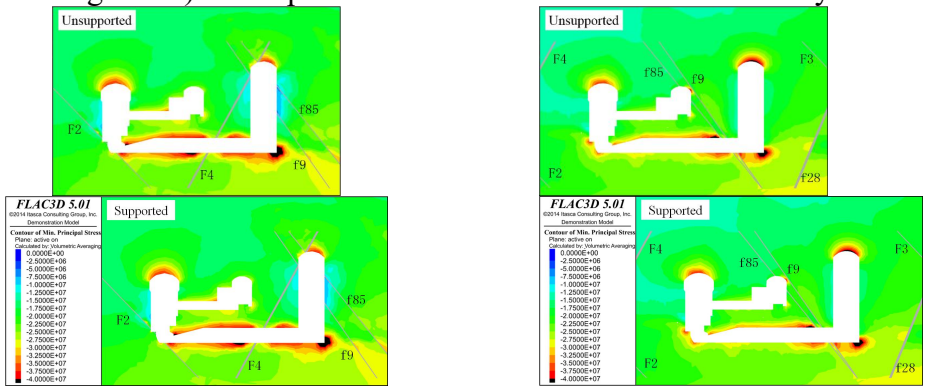

(a) unit 1# section(0+018.20m) (b) unit 4# section(0+111.80m)

Fig. 10 Distribution characteristics of σ_1 (unit: MPa) after the XI layer excavation

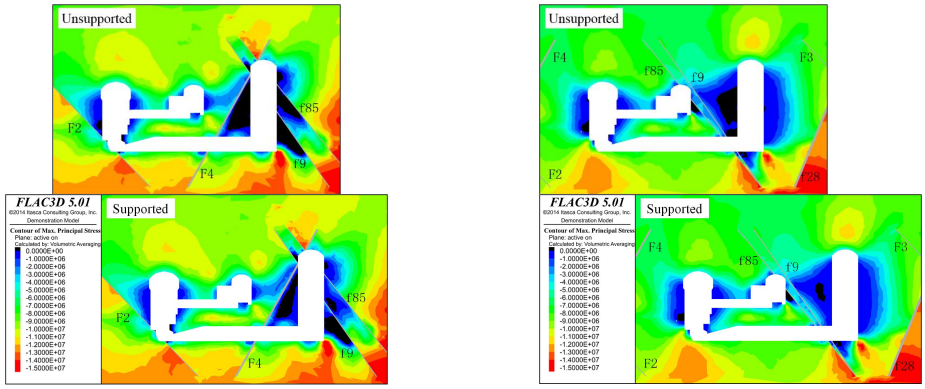

(a) unit 1# section(0+018.20m) (b) unit 4# section(0+111.80m)

Fig. 11 Distribution characteristics of σ_3 (unit: MPa) after the XI layer excavation

5.3 Relaxation damage zone of the surrounding rock

During the excavation process, the direction of maximum principal stress is roughly parallel to the cave wall, while the direction of minimum principal stress is roughly perpendicular to the cave wall. The maximum principal stress can be regarded as axial stress and the minimum principal stress as lateral stress. Figure 12 shows the distribution characteristics of crack closure ratio C3 after the VI layer and the XI layer excavation of the unit 1# section, and Figure 13 shows the distribution characteristics of the relaxation damage zone after the VI layer and the XI layer excavation of the unit 1# section which can be obtained from the relaxation damage zoning standard Tab.2. Figure 14 shows volume variation characteristics of cavern group surrounding rock relaxation damage area with excavation. From these figures, it can be seen that:

(1) With the progress of excavation, the area where the crack closure ratio C3 of the surrounding rock of the cavern group less than 0 gradually increases, and the distribution characteristics of the crack closure ratio C3 of the surrounding rock of the three major caverns before and after reinforcement are basically the same.

(2) The relaxation damage of the cavern is mainly concentrated in the high sidewall area of the main plant and the tail chamber, which is more influenced by the fault. In the unit 1# section, the range and depth of the weak and strong relaxation zones in the areas affected by fault F2, F4, f9 and f85 have increased significantly, and the damage zones mainly appear in the side walls of the main plant affected by fault F2 and the areas affected by fault f9 and f85 near the high side walls of the tail chamber.

(3) The volume of the weak relaxation zone, strong relaxation zone and damage zone of the underground cavern surrounding rock grows rapidly after the VI layer and the XI layer excavation, mainly related to the formation of high side walls in the main plant and tailing room, and the volume of the weak relaxation zone, strong relaxation zone and damage zone of the surrounding rock under the system support are all reduced compared with the unsupported working condition.

(4) In Fig.14, after the excavation of the cavern group, the volume of the weak relaxation zone under the unsupported condition is 1.377 × 106 m3, the volume of the strong relaxation zone is 1.240 × 106m3, and the volume of the damage zone is 0.181 × 106 m3. While the volume of weak relaxation zone under system support condition is 1.356 × 106 m3 (reduced by 1.50%), the volume of strong relaxation zone is 1.177 × 106 m3 (reduced by 2.25%), and the volume of damage zone is 0.080 × 106 m3 (reduced by 55.90%).

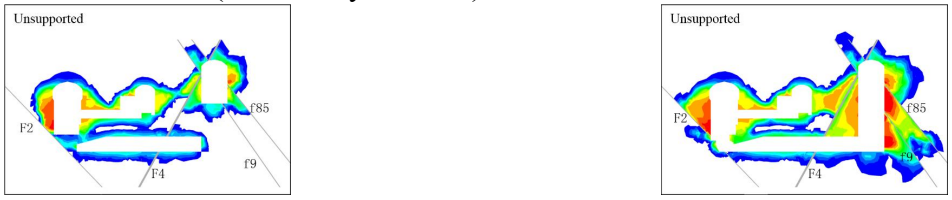

(a) after the VI layer excavation (b) after the XI layer excavation

Fig. 12 Characteristics of crack closure ratioC_3in the unit 1# section

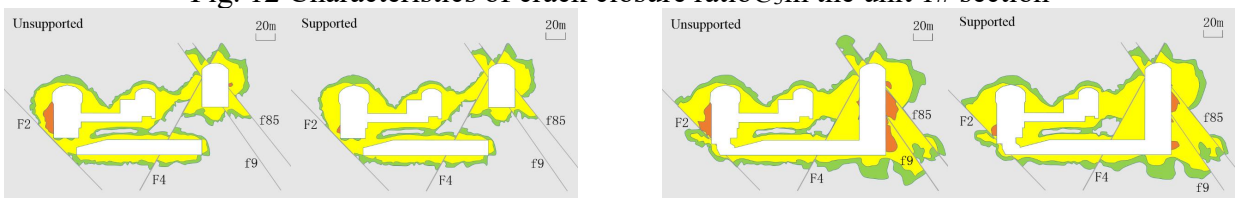

(a) after the VI layer excavation (b) after the XI layer excavation

Fig.13 Distribution characteristics of relaxation damage area in the unit 1# section

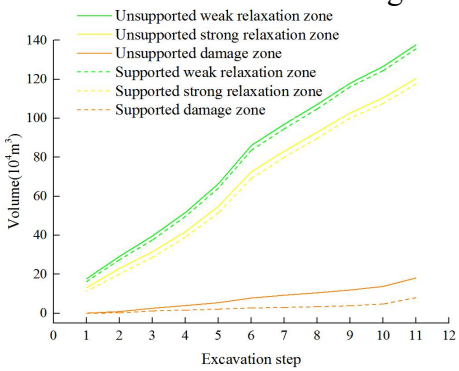

Fig. 14 Volume variation characteristics of surrounding rock relaxation damage area with excavation

6. Conclusions

The stress-crack strain evolution constitutive model was used to numerically simulate the excavation of the unsupported and systematically supported working conditions of Yebatan underground plant, and the surrounding rock displacement, stress and relaxation damage zone of the excavation at different levels were calculated. The following conclusions can be obtained:

(1) The displacement of the cavern surrounding rock increases with excavation step, and the deformation regulation of the underground cavern surrounding rock is consistent before and after reinforcement, and the deformation magnitude and range of the parts affected by fault F2, F4, f9, f85, f28, etc. are significantly increased, especially the range of the large deformation(more than 100mm) of the side walls of the main plant and the tail chamber are directly related to the fault, reflecting the obvious structural surface control type deformation characteristics.

(2) The volume of the high stress concentration area and tensile stress area in the surrounding rock of the three major caverns under the system supported working condition is reduced compared with the unsupported working condition. The high stress concentration area is distributed in the arch top of the plant, the tailwater connection hole, arch top and the bottom of the tail chamber. Tensile stress area is distributed in the side wall of main plant affected by fault F2, F4, f85, f28, and the side wall of tail chamber affected by F4, f9, f85, f28.

(3) The relaxation and damage zones of the cavern are mainly concentrated in the high sidewall area of the main plant and the tail chamber. In the unit 1#section, the range and depth of the weak and strong relaxation zones affected by fault F2, F4, f9 and f85 are significantly increased, and the damage zones mainly appear in parts of the sidewall of the main plant affected by fault F2 and the parts of the high sidewall of tail chamber affected by faults f9 and f85. Volume of the weak

relaxation zone, strong relaxation zone and damage zone of the surrounding rock under system support are all reduced compared with the unsupported condition.

References

[1] Brace W, Paulding Jr B, Scholz C. (1966) Dilatancy in the fracture of crystalline rocks. Journal of Geophysical Research, 71(16): 3939-3953.

[2] Peng J, Cai M, Rong G, Zhou C B and Zhao X G. (2015) Stresses for crack closure and its application to assessing stress-induced microcrack damage. Chinese Journal of Rock Mechanics and Engineering, 34: 1091-1100 (in Chinese)

[3] Corkum, A.G., and Martin, C.D.. (2007) The mechanical behaviour of weak mudstone (opalinus clay) at low stresses. International Journal of Rock Mechanics and Mining Sciences, 44, 196–209.

[4] David, E.C., et al. (2012) Sliding crack model for nonlinearity and hysteresis in the uniaxial stress–strain curve of rock. International Journal of Rock Mechanics and Mining Sciences, 52: 9–17.

[5] Liu H, Zhu C, Zheng K et al. (2021) Crack Initiation and Damage Evolution of Micritized Framework Reef Limestone in the South China Sea. Rock Mechanics and Rock Engineering, 54:5591-5601.

[6] Wen T, Liu Y, Yang C et al. (2017) A rock damage constitutive model and damage energy dissipation rate analysis for characterising the crack closure effect. Geomechanics and Geoengineering, 13:54-63.

[7] Mo Z, Qian L, Yao T, Gao Y, Xue F, Zhang J, et al. (2022) Unified transient creep constitutive model based on the crack evolution of micritic bioclastic limestone. PLoS ONE, 17: e0276100.

[8] Xu XL, Karakus M, Gao F et al. (2018) Thermal damage constitutive model for rock considering damage threshold and residual strength. J Cent South Univ, 25: 2523−2536.

[9] Qian L, Yao T Z, Mo Z G et al. (2022) Experimental study on crack evolution behavior and constitutive model of granite based on the deviatoric stress to peak strength ratio. Bulletin of Engineering Geology and the Environment, 81:278.

[10] Hoek E, Bieniawski Z. (1965) Brittle fracture propagation in rock under compression. International Journal of Fracture Mechanics, 1: 137-155.

[11] Scholz C. (1968) Experimental study of the fracturing process in brittle rock. Journal of Geophysical Research, 73: 1447-1454.

[12] Eberhardt E, Stead D, Stimpson B. (1999) Quantifying progressive pre-peak brittle fracture damage in rock during uniaxial compression. International Journal of Rock Mechanics and Mining Sciences, 36: 361-380.

[13] Cai M, Kaiser P K, Tasaka Y, et al. (2004) Generalized crack initiation and crack damage stress thresholds of brittle rock masses near underground excavations. International Journal of Rock Mechanics and Mining Sciences, 41:833-847.

[14] Qian L, Zhang J H, Wang X L et al. (2021) An Improved Creep Model for Granite Based on the Deviatoric Stress-to-Peak Strength Ratio. Arab J Sci Eng, 46: 5157-5170.

[15] Zhang G Y, Qian L, Zhang J H, Wang Z N and He J H. (2023) Study on the constitutive model and the identification of parameters of granite based on the crack closure ratio. J. Phys.: Conf. Ser, 2437 012090.